Polymer-based mesh as supports for multi-layered 3D cell culture and assays

Permanent link

http://nrs.harvard.edu/urn-3:HUL.InstRepos:12361260

Share Your Story

The Harvard community has made this article openly available.
Please share how this access benefits you. Submit a story .

Accessibility

Polymer-Based Mesh as Supports for Multi-layered 3D Cell Culture and Assays

Karen A. Simon, Kyeng Min Park[§], Bobak Mosadegh[§], Anand Bala Subramaniam[§],

Aaron Mazzeo, Phil M. Ngo and George M. Whitesides*

Department of Chemistry & Chemical Biology and

Wyss Institute for Biologically Inspired Engineering

Harvard University, Cambridge, MA 02138

[§] Contributed equally

*Corresponding author. Tel.: +1 617 495 9430; Fax: +1 617 495 9857.

E-mail address: gwhitesides@gmwgroup.harvard.edu (G.M. Whitesides)

Abstract

 Three-dimensional (3D) culture systems can mimic certain aspects of the cellular microenvironment found *in vivo*, but generation, analysis and imaging of current model systems for 3D cellular constructs and tissues remain challenging. This work demonstrates a 3D culture system – Cells-in-Gels-in-Mesh (CiGiM) – that uses stacked sheets of polymer-based mesh to support cells embedded in gels to form tissue-like constructs; the stacked sheets can be disassembled by peeling the sheets apart to analyze cultured cells—layer-by-layer—within the construct. The mesh sheets leave openings large enough for light to pass through with minimal scattering, and thus allowing multiple options for analysis—(i) using straightforward analysis by optical light microscopy, (ii) by high-resolution analysis with fluorescence microscopy, or (iii) with a fluorescence gel scanner. The sheets can be patterned into separate zones with paraffin film-based decals, in order to conduct multiple experiments in parallel; the paraffin-based decal films also block lateral diffusion of oxygen effectively. CiGiM simplifies the generation and analysis of 3D culture without compromising throughput, and quality of the data collected: it is especially useful in experiments that require control of oxygen levels, and isolation of adjacent wells in a multi-zone format.

1. Introduction

The field of tissue engineering has two major motivations: (i) to grow cells in constructs for replacement of organs, and (ii) to create experimental models of tissues (and, ultimately of organs and animals) for *in vitro* studies (e.g. in drug development, toxicology, pharmacokinetics, and radiation biology) that replace more expensive and more complex *in vivo* models [1]. 3D-culture models (organ slices [2], cellular spheroids [3-5], cells seeded or embedded in extracellular matrix (ECM) [6], cells grown in decellularized tissue scaffolds, artificial skin, microcarrier cultures [7])—with appropriate design—can mimic certain aspects of the native microenvironment of cells that can be difficult, if not impossible, to mimic in conventional 2D-culture systems [8]. These 2D-cultures lack a number of essential features required to mimic 3D tissues: i) 3D cell-cell and cell-ECM contacts that affect differentiation of cells; ii) 3D structural features that determine the mass transport-limited rates of molecules (e.g. oxygen, glucose, and carbon dioxide) required for the maintenance of the viability of cells *in vivo* to a surface from medium, and into tissues from capillaries; iii) 3D stromal tissues that support epithelial cells; (iv) 3D stratification of cells that enables co-culture and interaction of heterogeneous populations of cells; and (v) 3D mechanical stress that regulate behavior of cells in tissues (e.g. bone formation, wound healing, etc) [9-11].

In most tissues, cells are within a distance of $100 - 200$ μm from a blood vessel, and receive sufficient oxygen and glucose by passive diffusion from capillaries to maintain their metabolism [12, 13]. Beyond this distance, cells receive amounts of nutrients and molecules (oxygen in particular) that are too limited to allow normal, dioxygen-based metabolism [14, 15] and gene expression[16] that influence or determine progression of disease [16, 17]. Cancer cells that

populate the hypoxic (and often necrotic) central regions of the solid tumors, for example, exhibit stem cell-like properties, and resist both chemotherapy and radiotherapy [18].

Although current 3D cell culture systems allow monitoring of cellular response to different cues (for example, drugs, hormones, signaling molecules, nutrients and toxins, either in uniform concentrations or distributed in gradients in space and time); challenges in sample handling [1] and imaging [19] hinder the wide-spread use of these 3D-culture systems. Biological samples with moderate thickness, including cells cultured in 3D (< 1 mm thick) are commonly imaged using confocal microscopy [20]. Imaging by confocal microscopy, however, can be challenging because of limitations in optical depth of penetration, and photobleaching of dyes [19, 20]. Techniques that either modify the optics of the microscope (e.g. two-photon and multi-photon microscopy) [21-24], or acquire images of the samples from multiple angles (e.g. optical coherence (OCT) [25] and optical projection tomography (OPT)) [26], have been developed to overcome these limitations. These techniques, although successful in increasing the penetration depth of light into the samples, often sacrifice depth of field for resolution. Single (or selective) plane illumination microscopy (SPIM), which combines optical sectioning and tomography with confocal imaging, allows imaging of large samples at high resolutions and with minimal photobleaching [27]; but sample handling can be difficult, particularly with respect to the spatial control of the components within the thickness of 3D-culture models. Dissenroth and co-workers introduced a preparative technique called CLARITY to transform intact tissues into optically-transparent and molecularly-permeable constructs while preserving the native structure of these tissues. This method permits visualization of neurites over long distances and provide information on the topological morphology of traced neurons—information which is lost if specimens of the brain were sectioned mechanically [28].

Recently, we demonstrated that growing mammalian cells in thin (100 – 200 μm) slabs of paper-reinforced gel ("**C**ells-**i**n-**G**els-**i**n-**P**aper" or CiGiP), provided an experimentally simple approach with which to conduct *in vitro* 3D cell culture [29]. Hydrophobic patterns of wax were printed in arrays across the full thickness of cellulose paper to generate 96 hydrophilic zones that confined cells in circular slabs of ECM–based gels in the paper [30]. By stacking and de-stacking (e.g., peeling apart) sheets of cells embedded in hydrogels, CiGiP provided a simple approach for handling and analyzing cell cultures in 3D without requiring specialized equipment (most analysis can be done using a fluorescent gel scanner). The ease of separating stacked sheets of paper is in sharp contrast to the other methods required for analysis in other 3D cultures: microtomes, multi-photon microscopes, optical coherence tomography systems [20, 31], and laser–capture microdissection systems [32].

Although CiGiP simplifies handling and analysis of the cultured cells, the cellulose fibers that constitute paper scatter light (Fig. S-1A) and prevent high-resolution imaging of cells using an optical microscope. Many high-resolution techniques used routinely to analyze 2D cell cultures – for example, labeling with colorimetric stains to distinguish intracellular composition and structure, and observing cellular morphology through optical microscopy [20] – therefore cannot be applied directly to CiGiP cultures. Another limitation of CiGiP cultures, as described by Derda *et. al.* [30], is that the wax-printed barriers allow dioxygen (O_2), and we presume, other molecules (certainly CO_2, hydrophobic drugs (e.g. calcein-AM, mitomycin C) and perhaps water-soluble molecules such as glucose) to diffuse laterally within the plane of the sheet from the sides of the stacked 3D constructs. The diffusion of oxygen from the sides allowed cells to survive along the rims of the cell culture zones, even in layers that should, in principle, be severely depleted of oxygen [30].

Here we describe a modification of CiGiP– "**C**ells-**i**n-**G**els-**i**n-**M**esh" or (CiGiM) – for generating 3D tissue models in which we replace the paper in CiGiP with an open polymer mesh as a scaffold to support cells embedded in ECM-based gels. Openings in the mesh (Fig. S-1B) allow unimpeded observation of cells by light microscopy, and high-resolution imaging by confocal microscopy. In CiGiM, we also demonstrate the value of decal transfer to fabricate hydrophobic barriers based on paraffin wax; these decal-transferred barriers are much more effective than the wax-printed barriers used in CiGiP for blocking the mass transport of O_2 by diffusion from the periphery of the individual zones of the cell culture scaffolds.

2. Materials and Methods

2.1 Materials

Reagents and chemicals were obtained from Invitrogen unless otherwise indicated. MDA-MB-231 cells, Eagle's Minimum Essential Medium (EMEM), and trypan blue were purchased from American Type Culture Collection (ATCC). Glutamax^{TM} and penicillin-streptomycin solution were obtained from Gibco. Polybrene was acquired from Sigma. Parafilm$^{®}$ was purchased from VWR, and polyethylene(terephthalate) (PET) mesh was purchased from McMaster-Carr. Paraformaldehyde was from Electron Microscopy Sciences.

2.2 Cell Culture and Transfection

We cultured MDA-MB-231 breast cancer cells as recommended by ATCC in Eagle's Minimum Essential Medium (EMEM) at pH 7.2 with fetal bovine serum (10% (v/v)), 1% Glutamax^{TM} (1% (v/v)), and penicillin-streptavidin (1% (v/v)). We maintained cells as adherent cultures in vented tissue culture flasks at 37 ºC and 5% CO_2. To express green fluorescence

protein, the cells were transfected by lentivirus (GFP) in the presence of 5 mg/mL polybrene as described previously by Mammoto *et. al.* [33].

2.3 Preparation of Multi-zone PET-Based Mesh Sheets

2.3.1 Fabrication of Multi-zone Mesh Sheet

PET-based mesh sheets were placed on a glass plate inside a SPI Plasma Prep II Chamber (Structure Probe Inc., West Chester, PA).We exposed the mesh to air plasma (100 W, ~1500 mTorr) for 30 minutes on each side. We created the desired pattern in the Parafilm® by pressing a custom-made steel-rule die (Apple Steel Rule Die. Co., Milwakee, WI) against the film with a pneumatic press (Tippmann Clicker 1500). Adobe Illustrator CS4 files of the design of the steel-rule die are available by request. We sandwiched the Parafilm® decal and mesh between two aluminum plates. Using a hydraulic press with a heated platen (55 °C), we pressed the aluminum plates with sufficient pressure (~5000 psi) for no more than 20 seconds (Fig. 1A). Upon releasing the pressure from the hydraulic press, we retrieved the multi-zone mesh with Parafilm® barriers generated by forcing the decal into the mesh.

2.3.2 Sterilization of the mesh.

We immersed the multi-zone mesh sheets in ethanol (200 proof) for 1 hour. Mesh sheets were then air-dried and exposed to UV light inside a laminar flow hood for another hour. Air-dried samples were stored in a dry Petri dish, sealed with a strip of stretched Parafilm®.

2.4 Fabrication of Multi-zone Paper-Based Supports

Multi-zone paper-based supports were prepared as described by Derda *et. al.*[30]. In brief, multi-zone designs were drawn in Illustrator CS4 (Adobe) and printed to a sheet of Whatman #114 paper (20 cm × 20 cm) by a wax printer (Phaser 8560DN, Xerox). We baked the wax-printed paper in an oven to melt and allow wax to penetrate through the thickness of the paper. The wax-printed paper was cut to multi-zone plates using a laser cutter (Versa Laser-Universal Laser VL-300). We immersed the baked multi-zone paper in ethanol for 1 hour to remove the residual wax. The paper was incubated with a fresh solution of ethanol for an additional hour, and air-dried in a laminar flow hood with UV light for 1 hour for sterilization.

2.5 Seeding of Cells onto Multi-zone Mesh Sheets and Multi-zone Paper-based Supports

We detached the cells from the tissue culture flasks by incubating in a solution of trypsin-EDTA for 5 minutes and washing in culture media. We resuspended the cells in Matrigel (BD) at a concentration of 4×10^7 cells/mL Matrigel, or diluted them to obtain the desired concentrations to prepare the calibration curve. For all suspensions, we used Matrigel as received without further dilution. While holding the multi-zone mesh with tweezers, we applied the suspension on the hydrophillized zones of the mesh using a micropipette. Using the tip of the micropipette, we spread the suspension on the zone to allow complete permeation of the mesh in the zone by the cells in Matrigel. Unless noted otherwise, we applied 3 μL of the 4×10^7 cells/ mL Matrigel suspension on each zone. Based on this volume and concentration, the initial seeding density in each zone was 1.2×10^5 cells/zone. After seeding, we placed the mesh in a Petri dish containing medium that was pre-warmed to 37 ℃. To allow the Matrigel to gel completely, we incubated

the multi-zone mesh, or paper containing suspensions of cells, in Matrigel for at least 12 hours, prior to stacking.

2.6 Culture of Stacked CiGiM

To keep the sheets in conformal contact and submerged in culture medium, we sandwiched layers of paper or mesh containing cells embedded in Matrigel in a poly(acrylonitrile butadiene styrene (ABS)-based holder, or in between two metal plates (Fig. S-3). These holders were custom-made with holes corresponding to the positions and diameters of the zones of the multi-zone mesh. The plates were also equipped with four threaded holes that fit screws to guide the alignment and fastening of the sheets during stacking. Using these holders, we stacked and secured the sheets in place with the screws and the appropriate nuts until they were finger-tight. We placed the stacked cultures in a Petri dish containing culture media. Each stack was cultured for 9 days and media was changed every 2 days.

2.7 Analysis of Cell Viability and Imaging

To evaluate viability, we disassembled the holders and peeled the layers apart with tweezers. The separated layers were washed briefly with warm (37 ºC) Hank's Balanced Saline Solution (HBSS) for 5 minutes, stained with calcein (4 μg/mL) in HBSS for 20 minutes at 37 ºC and washed twice with HBSS (20 ºC) before scanning for the intensity of calcein. We used Typhoon FLA 9000 gel scanner, set at a resolution of 50 μm and a photomultiplier tube (PMT) setting of 300 V to image for the intensity of calcein. The intensities of the zones were quantified using ImageJ. The number of cells in each zone was calculated using a calibration curve prepared by measuring the intensity of calcein staining in known number of cells (Fig. S-6A).

To label dead cells, we incubated the layers of the constructs in trypan blue (ATCC, 0.2% in PBS (1X), pH 7.2) for 10 minutes. After washing the stained solutions in PBS (twice for 5 minutes), we viewed each layer under an inverted light microscope.

Layers to be examined by confocal fluorescence microscopy were washed in PBS and fixed in 4% aqueous paraformaldehyde (PFA) overnight, washed twice with PBS, incubated in DAPI (30 nM in PBS) for an hour, and washed twice with PBS to remove excess dye before microscopy. We viewed the cells in the zones of each layer using a Zeiss LSM710 confocal microscope (Carl Zeiss Microscopy, LLC, Thornwood, NY).

3. Results and Discussions

Building on our previous work on paper-based cell culture, we start with the premise that our 3D mesh-sheet based cultures should be designed with five features: (i) The multi-zone mesh sheets should consist of two distinct regions: hydrophilic zones that allow seeding of cells embedded in ECM (i.e. Matrigel), and hydrophobic barriers that confine the seeded cells within the boundaries of the hydrophilic zone. (ii) The cell-culture platform should consist of materials (e.g. mesh fibers, hydrogels, and hydrophobic barriers) that are all non-toxic to cells. (iii) The film and polymer-based mesh should consist of materials which withstand chemical, thermal, or UV sterilization procedures. (iv) The polymer-based mesh sheets should consist of a material which is either hydrophilic or can be made hydrophilic to facilitate spreading and wicking of liquid ECM through the thickness of the mesh. (v) The mesh sheet should be of a total thickness that does not limit the mass transport of O_2 and other nutrient molecules (e.g., glucose), or waste products (e.g., CO_2, or lactate), within a single sheet, at a typical seeded cell concentration (< 200 μm for ~100,000 cells/μL) [34].

3.1 Materials for Creating Multi-zone Mesh.

We chose mesh because it has the properties of paper—it is stackable and wettable—which are attractive as a supporting scaffold for multi-layered 3D cultures. Unlike paper, mesh has openings large enough for microscopy without scattering of light.

We seeded and gelled suspensions of MDA-MB-231 cells in Matrigel on several commercially available mesh sheets—poly(propylene), Nylon, PEEK, and poly(ethylene terephthalate) (PET)—to identify materials that would hold the Matrigel most stably. Among the various mesh materials we tested, PET and PEEK provided the best performance in their ability to support the gel-suspended cells. We found that gels supported on other mesh materials tended to fall off from the mesh during culture (Figure S-2). Although we infer that adhesion between the surface of the mesh and the gel is important, it is unclear why PET and PEEK proved superior to other polymers for supporting hydrogels; we speculate that the aromatic groups of these materials oxidized on exposure to the plasma that was used to render the surface wettable, to give a greater density of polar groups. Although both PET and PEEK supported the gels stably; PET is significantly less expensive than PEEK, and therefore we chose it as the mesh material for all of the experiments described in this paper. We used a PET mesh that is commercially available at a thickness comparable to Whatman #114 chromatography paper (~180 μm), which we used previously for CiGiP [30]. The PET-based mesh also had openings with diameters (250 μm) large enough to visualize the cells through a microscope. We did not optimize the ratio of the dimensions of the opening of the mesh and the fiber diameters in this work.

We chose Parafilm® as the hydrophobic film with which to fabricate the barriers on the mesh. Parafilm® (a film composed of approximately 50/50 paraffin wax and polyolefin) is inexpensive,

has a thickness of less than 200 μm (~127 μm), and can be heated and solidified reversibly without changing its chemical and bulk properties [35]; these characteristics make it a suitable material to serve as a hydrophobic barrier. Its fabrication into decals to make "zones" is straightforward.

3.2 Hydrophilization of PET-Based Mesh Sheets

Spreading aqueous hydrogels on unmodified polymeric meshes proved difficult. Instead of spreading and forming films that spanned the voids of the mesh, the liquid ECM beaded on native polymer fibers and formed drops, an observation that we attribute to the hydrophobicity (e.g. high contact angle of the aqueous solution of the gel) of the native polymers. We overcome this limitation by rendering our meshes hydrophilic.

We measured the apparent contact angle of water on the mesh sheets (the droplets were large enough that they rested both on the fibers and on air in the voids of the mesh, and hence we do not measure the equilibrium contact angle of the polymer) before and after hydrophilization using a modified Sessile-Drop Technique [36, 37]. The full details of the measurement procedure are provided in the Supplemental Information. Of the three methods we tested – treatment with air plasma, base hydrolysis, or acid hydrolysis – treatment with air-plasma reduced the apparent contact angle of water on the polymeric material the most—from 113 ± 3 to 23 ± 3 (See Table S-1 for contact angles). Plasma treatment also required the shortest treatment time (approximately 60 minutes to air plasma).

3. 3 Fabrication of Multi-zone Mesh Sheets

Figure 1A shows the two-step decal-transfer process we employed to create multi-zone mesh sheets. This process combines (i) steel-rule die cutting and (ii) hot pressing. First, we fabricated hydrophobic decals by pressing a custom-made steel-rule die against sheets of Parafilm®. The steel-rule die was designed to punch out a square array of 25 circular zones (5×5) with a diameter of about 6 mm in the Parafilm®. The zones have diameters that are similar to those of the wells in standard 96-well plates, but we used a smaller, 25-well design, to minimize the use of media and reagents. Second, we hot-pressed the Parafilm® decals onto PET meshes treated with air plasma in between two aluminum plates heated to 55 °C (Fig. 1A). The Parafilm® melted and filled the voids of the mesh to form a solid barrier extending across the full thickness of the mesh.

We attempted to pattern sheets of paper by embossing Parafilm® decals; we found that the Paraffin failed to penetrate the full thickness of the paper. In the mesh, voids are shaped regularly and span the thickness of the sheet; this geometry allows the molten paraffin to penetrate the voids efficiently. In paper, the structure of the voids is non-uniform and irregularly oriented in space, and it is thus difficult for the molten paraffin decals to block the voids effectively. To render uniform hydrophobic barriers, as described previously, we printed the sheets of paper with hydrophobic wax, and then baked these sheets of paper to allow the wax to permeate the entire thickness of the paper [30].

We sterilized the multi-zone mesh sheets by immersing the sheets in ethanol for an hour, and then exposing the sheets to UV light for 24 hours. Although it was possible to autoclave the multi-zone sheets using the "liquid setting" (i.e. autoclave the sheets while immersed in water), soaking each sheet in separate containers was necessary to prevent the mesh sheets from

sticking together (Parafilm® barriers stick together when molten); thus made the process of sterilization time-consuming.

3.4 Generation of 3D Cultures on the Zones of Patterned Sheets of Mesh and Paper

Figure 1B describes the generation of multi-zone CiGiM and CiGiP. We constructed 3D cultures of cells using single sheets of the multi-zone mesh and paper by spotting suspensions of MDA-MB-231-GFP cells in cold, liquid Matrigel (4 °C) onto the zones of the mesh or paper. The Matrigel transforms from a liquid to a gel inside the mesh or paper when immersed in warm culture media (37 °C).[29, 30] We cultured the sheets as single layers (SL), or stacked multiple sheets in a custom-built holder to generate thicker constructs (Fig. S-3); holders were either fabricated using 3D-printing (ABS-based holders) or machined (stainless steel plates). Although liquid Matrigel gels rapidly when heated to temperatures that range from 22 °C to 35 °C [38], out of an abundance of caution, we waited for at least 12 hours before stacking to ensure that the Matrigel had gelled completely.

3.5 Comparison of the Characteristics of Multi-zone Mesh Sheets and Paper

Figure 1C shows representative photographs of the multi-zone mesh and paper. Fibers of the mesh sheets are arranged and spaced regularly; openings in the mesh span the thickness of the layer. Paper appears opaque, with the cellulose fibers providing no voids large enough to span the thickness of the sheet. Micrographs show noticeable differences in the structure of the wax-printed and decal-transferred barriers (Fig. 1 C, inset). Paraffin decals filled the voids within the mesh, whereas the printed wax only coated the fibers of the paper, with open pores in the hydrophobic region visible from the filtering of light through the wax-coated fibers. We thus

hypothesized that decal-transferred Parafilm® barriers would block the lateral diffusion of molecules (including oxygen) in the plane of the film more effectively than wax-printed barriers, since there were fewer apparent macroscopic pores in the hydrophobic regions.

3.6 PET-based mesh supports permit visualization of cells in gels with optical microscopy.

We spotted suspensions with different concentrations of MDA-MB-231-GFP cells (6×10^4 cells/ zone to 30×10^4 cells/ zone) into zones of paper and mesh. The increase in the number of these MDA-MB-231 cells can be distinguished clearly by the bright-field images of the zones of the mesh. In contrast, all bright-field images of the zones of paper that contained cells-in-gels showed only networks of cellulose fibers (Fig. 2). These results illustrate one of the advantages of using mesh as a support for 3D cultures: it is possible to observe both the density and the morphology of the non-labeled cultured cells using an optical microscope.

Since differences in the density of cells cultured on the paper sheets were indistinguishable with bright-field microcopy, we stained the zones of multi-zone mesh and paper with calcein, and acquired images with a fluorescence gel scanner. Intensities of the zones increased linearly with increasing concentrations (Fig. S-4C) of cells for both mesh and paper—an observation consistent with our previous work on multi-layered 3D cell culture supported on sheets of chromatography paper [30]. Thus, cells-in-gels cultured on paper and mesh can both be analyzed using a fluorescence scanner; the ease of use, and ready availability of scanners, provided a means of comparing the two patterning methods (i.e. wax printing of chromatography paper, and decal transfer of Parafilm® onto mesh) directly in their ability to block O_2.

3.7 Decal-transferred Parafilm® reduced the diffusion of O_2 from the rims of the barriers to the zones of the multi-zone mesh

To identify the patterning method that blocks the lateral diffusion of oxygen more effectively, we assembled, in parallel—two stacks—(i) nine layers of multi-zone mesh sheets, and (ii) nine layers of multi-zone paper, both containing suspensions of MDA-MB-231-GFP cells in Matrigel. For convenience, we refer to these layers as L1, L2, L3, L4, L5, L6, L7, L8, and L9, where L1 is the topmost layer, and is in contact with the medium. Stacking these sheets on top of a sheet of cellulose acetate (L9 is in contact with this sheet) allowed us to generate multi-layered 3D cultures. The oxygen-impermeable cellulose acetate sheet blocked access of O_2 from the bottom of the stack. In the stack of multi-zone sheets of paper, a sheet of perforated cellulose acetate, with perforations aligned with the zones containing the cells, limited the diffusion of media and gases to the hydrophobic regions of the topmost layer of the stack (Fig. 3A). Following established protocols from CiGiP [30], we also placed a sheet of perforated cellulose acetate on top of the stack of multi-zone sheets of mesh. In this stacked configuration, we expect the concentration of O_2 to decrease monotonically from the top (i.e. in L1) to the bottom (i.e. L9) of the stack (Fig. 3A) [29, 30]. The stacks were held together with custom-built (using 3D printing, dimensions and fabrication method described in detail in the supporting information), rigid polymeric holders fabricated from poly(acrylonitrile butadiene styrene) (ABS) (Fig. S-3A).

After nine days of culture, we disassembled the stacks by disassembling the holder, peeling the layers apart, incubating each layer in a solution of calcein-AM, and acquired fluorescence (calcein generated from the hydrolysis of calcein-AM—a reaction that is catalyzed by intracellular esterases of viable cells) [39] images of each layer with a fluorescence gel scanner. We found that for both systems (paper and mesh), the intensity of calcein in the zones decreased

monotonically from L1 to L9 (Fig 3C, D). These results are consistent with our earlier work, in which cell viability decreased from the top to the bottom of the stack [29, 30].

In layers where O_2 was more limited than in L1 (i.e. L2 to L9), the distribution of calcein intensities within individual zones was heterogeneous in paper, but relatively homogeneous in mesh (Fig. 3C). In paper, calcein intensities were higher around the rims than the cores of the zones (imaged as dark rings); in mesh, the intensities were uniform within individual zones. We interpret the formation of rings of live cells as the result of cells migrating to the edges of the zones to regions of higher relative oxygen concentrations within the lateral confines of a single sheet [29, 30]. To compare the distribution of the florescence intensity within the zones, we obtained a line profile of calcein fluorescence intensities across the diameter of representative zones, and generated intensity plots for mesh and paper. The intensity plots confirmed concentration of cells (shown as two "peaks") at the edge of the zones of paper; these peaks were absent in the zones of mesh (Fig. 3E). This difference confirmed that completely filling the voids of the mesh reduced the lateral diffusion of O_2 sufficiently that it prevented the formation of rings consisting of live cells at the rim of the zones.

3.8 Colorimetric staining and imaging using light microscopy

Since using mesh as a support allowed viewing of the cultured cells with light microscopy, it was also possible to use colorimetric histological stains to assess cell death. We found that the uptake of the dye in the cells increased from L1 to L9 (Fig. S-5A), when the cells were stained with trypan blue (this dye only permeates the membranes of dead cells) [40]. These results confirmed that cell death increased in deeper layers that received less O_2, and is consistent with the results obtained from staining with calcein (Fig. 3C, 3D). In the multi-zone paper,

trypan blue stained both the cells and the fibers (Fig. S-5A), and hence correlating fluorescence and colorimetric staining for cells in paper was not possible. These results show that the use of mesh as a support for 3D cultures, made it possible to evaluate the viability of cells in 3D using simple equipment and reagents, such as optical microscopes and colorimetric stains.

3.9 Further reduction of O$_2$ diffusion in stacked CiGiM cultures and high-resolution imaging

Despite the fact that CiGiM eliminated the 'rings of live cells' observed with CiGIP, measurements of intensity indicated that cells in L9 did not die completely in stacks of either mesh or paper (Fig. S-3A); we hypothesized that the pores in the 3D-printed ABS holders might have allowed small amounts of oxygen to diffuse into the cultures. We further optimized the culture conditions in the next sets of experiments. To reduce oxygen diffusion into the stacked culture, we replaced our ABS holders with machined stainless steel plates as holders to bring the layers of the mesh into conformal contact. We also wrapped the periphery of the stack with a strip of Parafilm® (Fig. S-3B).

After nine days of culture, we de-stacked the layers, stained with calcein, and scanned the layers with a fluorescence scanner as described previously. We then fixed the cells with paraformaldehyde (PFA, 4% by volume in phosphate buffered saline, PBS) to preserve the cell's ultrastructure. Using standard protocols, we stained the cells in the sheets with fluorescent stain, 4', 6-diamidino-2-phenylindole (DAPI) to visualize nuclei. Figures 4A and 4B show high-resolution, confocal fluorescence images of cells cultured on mesh-based supports. Green fluorescence allowed visualization of the morphology of the cells that expressed GFP, while blue fluorescence from DAPI labeled the nuclei of all cells. The intensity of GFP in the cells decreased continuously from L1 to L7, and became undetectable in L8 and L9 (Figs. 4A, S5-B).

These results were consistent with results from staining with calcein (Fig. 3C) and optical microscopy (Fig. S5-A). Since GFP has a half-life anywhere between 10 to 26 hours post-cell death [41], this protein is likely degraded completely in cells that have been dead for more than 24 hours prior to fixing. This degradation explains the decrease in GFP fluorescence in deeper layers of the stack.

The morphology of the cells transitioned from spindle-shaped in the upper layers to round in the lower layers; this change in shape further suggests that the cells in the upper layers were predominantly alive, while cells in the lower layers were mostly dead. Using a calibration curve (Fig. S-6A), we quantified the number of viable cells from the fluorescence signal of calcein (Fig. 4C), and found that the number of viable cells decreased by up to 96% Eq. (1).

$$\% \text{ decrease} = \frac{(\text{number of viable cells in } L_1 - \text{number of viable cells in } L_N) \times 100}{(\text{number of viable cells in } L_1} \quad \text{(Eq. 1)}$$

This result confirmed that non-porous materials, (here, the stainless steel plates and a strip of Parafilm® at the edge of the stack), provided uniform pressure, kept the stack of mesh sheets intact, eliminated diffusion of oxygen to the cells from the edge of the stack, and achieved virtually complete cell death at the bottom layers.

3.10 The depletion of oxygen in the lower layers of CiGiM cultures was primarily due to the consumption of oxygen by cells in the upper layers

Having established that CiGiM was able to produce one-dimensional gradients in oxygen, and presumably, of other nutrients such as glucose throughout the thickness of the construct, we proceeded to analyze the distribution of cells cultured in CiGiM. The number of viable cells continuously decreased from L1 to L9. In L1, the number of cells exceeded the initial seeding density by five-fold, while in L2 the number of cells remained roughly similar to the initial

seeding density. In lower layers, the number of viable cells after nine days of culture was below the number of cells seeded initially. In a given mesh layer, the number of cells can increase due to the proliferation of the cells, or migration of cells into the layer from other layers, and can decrease due to cell death, or migration of cells from the layer into other layers (Fig. 4C).

Clearly, cells in deeper layers of the stack, depleted of nutrients, died or migrated to upper layers. The depletion in nutrients could be due to two potential, and possibly coupled, reasons: (i) the cells on the topmost layer consumed most of the O_2 (ii) the Matrigel and mesh were barriers to the diffusion of oxygen from the nutrient-rich media and thus the cells received decreasing fluxes of O_2 the further they were from L1.

To evaluate how these two factors influence the distribution of cells in CiGiM, we stacked sheets of the mesh containing Matrigel that were devoid of cells, except for in a single layer. We seeded respectively, cells in L2, L3, and L4 while always keeping L1 devoid of cells (Fig. 5). Figures 5B and 5C show that the cells seeded in deeper layers proliferated above the initial seeding density, which suggested that they received adequate O_2 and nutrients when there were no cells in L1. These experiments showed clearly that the consumption of O_2 by cells in L1 in conventional CiGiM constructs, accounted for the most of the depletion in nutrients, and hence cell death, in the lower layers. These experiments also revealed, however, that cells migrated toward the upper layers, despite the fact that there were no cells in L1; this migration indicates that there was a gradient in the availability of nutrients due to the distance between the cell-containing layers and the nutrient-rich media. The further the cells were from the oxygenated medium, the greater the cells migrated to the upper layers; this observation is consistent with our earlier observation that cells migrate preferentially to nutrient-rich and O_2-rich regions.

4. Conclusion

This paper describes a new method to pattern hydrophobic barriers by hot pressing a paraffin-based decal onto a hydrophilic polymeric mesh. This approach covers completely the voids in the mesh and thus eliminates the lateral diffusion of O_2 from the sides of the stacked 3D constructs that previously complicated the interpretation of analogous experiments using other designs and procedures [29, 30]. We have also demonstrated that this 3D culture approach permits layer-by-layer analysis and visualization of cells at micrometer-scale resolution by using stacks of patterned polymer-based mesh sheets as supports for hydrogel-embedded cells. Since cells in mesh-based supports can be visualized directly with a light microscope, colorimetric stains can be used to stain the ECM (e.g. laminin to stain collagen) and the cells (e.g. Trypan Blue to stain dead cells; hemotoxylin and eosin to stain nuclei and cytoplasm). Simple experiments on 3D cultures can therefore be conducted even if a fluorescence gel scanner or a fluorescence microscope are unavailable. CiGiM is probably suited for time-lapse tissue culture experiments, since cells can be viewed progressively without fixation and staining.

We note two limitations of CiGiP—(i) mesh sheets, at the present level of development, lack mechanical support needed to prevent some of the Matrigel slab containing cells from falling out of the holes in the mesh with fluid flow or mechanical agitation. We expect that using mesh with smaller openings will provide better support, but may compromise ease of visualization with a light microscope; (ii) the fabrication of the multi-zone mesh sheets was more time-consuming, and required more steps (i.e. hydrophilization of PET-based mesh, two-step decal transfer) than wax-printed multi-zone paper. The choice between wax printing and decal transfer of paraffin films for creating multi-zone patterns would depend on the application; wax printing offers the

advantage of simplicity and rapid fabrication, while decal transfer of Parafilm® blocks O_2 efficiently, and controls the flux of nutrients from upper layers to lower, more efficiently.

We believe that CiGiM will provide life and biomedical scientists a useful new platform for *in vitro* tissue models and cell-based assays. This platform can be assembled and analyzed reliably and simply. CiGiM, for example, seems very well adapted for screening drug candidates for chemotherapeutic agents, or for evaluating the efficacy of drugs on tumor cells with different levels of hypoxia. We anticipate that multi-zone mesh sheets makes it possible to isolate cancer cells cultured in hypoxic regions (i.e., from bottom layers of the stack); these hypoxic cancer cells are hypothesized to exhibit stem cell-like properties and are more resistant to chemotherapeutic drugs than cells cultured in normoxic conditions [18]. In intact tumors, these cells are believed to reside on the core of malignant tumors, and CiGiM may serve as an *in vitro* tumor model to determine whether candidate drugs can kill these resistant cells.

Acknowledgements

References

1.   Griffith LG, Swartz MA. Capturing complex 3D tissue physiology in vitro. Nat Rev Mol Cell Biol. 2006;7:211-24.

2.   Toda S. A new organotypic culture of thyroid tissue maintains three-dimensional follicles with C cells for a long term. Biochem Biophys Res Comm. 2002;294:906-11.

3.   Timmins NE, Hardling FJ, Smart C, Brown MA, Nielsen LK. Method for the generation and cultivation of functional three-dimensional mammary constructs without exogenous extracellular matrix. Cell Tissue Res. 2005;320:207-10.

4.   Kelm JM, Timmins NE, Brown CJ, Fussenegger M, Nielsen LK. Method for generation of homogeneous multicellular tumor spheroids applicable to a wide variety of cell types. Biotechnol Bioeng. 2003;83:173-80.

5.   Castaneda F, Kinne RKH. Short exposure to millimolar concentrations of ethanol induces apoptotic cell death in multicellular HepG2 spheroids. J Cancer Res Clin Oncol. 2000;126:305-10.

6.   Zegers MMP, O'Brien L, Yu W, Datta A, Mostov KE. Epithelial polarity and tubulogenesis in vitro. Trends Cell Biol. 2003;13:169-73.

7.   Kim JB. Three-dimensional tissue culture models in cancer biology. Semin Cancer Biol. 2005;15:365-77.

8.   Cushing MC, Anseth KS. Hydrogel Cell Cultures. Science. 2007 May 25, 2007;316(5828):1133-4.

9.   Bhadriraju K, Chen CS. Engineering cellular microenvironments to improve cell-based drug testing. Drug Discovery Today. 2002;11:612-20.

10.   Bissel MJ, Radisky DC, Rizki A, Weaver VM, Petersen OW. The organizing principle: microevironmental influences in the normal and malignant breast. Differentiation. 2002;70:537-46.

11.   Bissell MJ, Hall HG, Parry G. How does the extracellular matrix direct gene expression? J Theor Biol. 1982;99:31-68.

12.   Jain RK, Au P, Tam J, Duda DG, Fukumura D. Engineering vascularized tissue. Nat Biotech. 2005;23(7):821-3.

13.   Folkman J, Hahnfeldt P, Hlatky L. Cancer: looking outside the genome. Nat Rev Mol Cell Biol. 2000;1:76-9.

14.   Schumacker PT, Samsel RW. Analysis of oxygen delivery and uptake relationships in the Krogh tissue model. J Appl Physiol. 1989;67:1234-44.

15.   Eichelbronner O, D'Almeida M, Sielenkamper A, Sibbald WJ, Chin-Yee IH. Increasing P50 does not improve Do2 CRIT or systemic Vo2 in severe anemia. Am J Physiol. 2002;283:H92-H101.

16.   van PJF, van MH, Nevens F, Verslype C. Chronic hypoxia emerging as one of the driving forces behind gene expression and prognosis of hepatocellular carcinoma. ISRN Pathol. 2011:273924-34, 10 pp.

17.   Dewing D, Emmett M, Pritchard JR. The roles of angiogenesis in malignant melanoma: trends in basic science research over the last 100 years. ISRN Oncol. 2012;2012:546927, 7 pp.

18.   Brown JM, Wilson WR. Exploiting tumour hypoxia in cancer treatment. Nat Rev Cancer. 2004;4:437-47.

19.   Pampaloni F, Reynaud EG, Stelzer EHK. The third dimension bridges the gap between cell culture and live tissue. Nat Rev Mol Cell Biol. 2007;8:839-45.

20.   Smith LE, Smallwood R, Macneil S. A comparison of imaging methodologies for 3D tissue engineering. Microsc Res Tech. 2010;73:1123-33.

21.   Centonze VE, White JG. Multiphoton excitation provides optical sections from deeper within scattering specimens than confocal imaging. Biophys J. 1998;75:2015-24.

22.   Gilbert RJ, Hoffman M, Capitano A, So PTC. Imaging of three-dimensional epithelial architecture and function in cultured CaCo2a monolayers with two-photon excitation microscopy. Microsc Res Tech. 2000;51:204-10.

23.   Gobel W, Kampa BM, Helmchen F. Imaging cellular network dynamics in three dimensions using fast 3D laser scanning. Nat Methods. 2007;4:73-9.

24.   Zipfel WR, Williams RM, Webb WW. Nonlinear magic: multiphoton microscopy in the biosciences. Nature Biotech. 2003;21:1369-77.

25.   Huang D. Optical coherence tomography. Science. 1991;254:1178-81.

26.   Sharpe J. Optical projection tomography as a tool for 3D microscopy and gene expression studies. Science. 2002;296:541-5.

27.   Stelzer EHK, Lindek S. Fundamental reduction of the observation volume in far-field light microscopy by detection orthogonal to the illumination axis: confocal theta microscopy. Opt Commun. 1994;111:536-47.

28.   Chung K, Wallace J, Kim S-Y, Kalyanasundaram S, Andalman AS, Davidson TJ, et al. Structural and molecular interrogation of intact biological systems. Nature. 2013;497:332-7.

29.   Derda R, Laromaine A, Mammoto A, Tang SKY, Mammoto T, Ingber DE, et al. Paper-supported 3D cell culture for tissue-based bioassays. Proc Natl Acad Sci USA. 2009;106:18457-62.

30.   Derda R, Tang SKY, Laromaine A, Mosadegh B, Hong E, Mwangi M, et al. Multizone paper platform for 3D cell cultures. PLoS One.6:e18940.

31.   Graf B, Boppart S. Imaging and analysis of three-dimensional cell culture models. In: Papkovsky DB, editor. Live Cell Imaging: Humana Press; 2010. p. 211-27.

32.   Espina V, Wulfkuhle JD, Calvert VS, VanMeter A, Zhou W, Coukos G, et al. Laser-capture microdissection. Nat Protocols. 2006;1:586-603.

33.   Mammoto A, Connor KM, Mammoto T, Yung CW, Huh D, Aderman CM, et al. A mechanosensitive transcriptional mechanism that controls angiogenesis. Nature. 2009;457:1103-8.

34.   Hrabětovà S, Nicholson C. Biophysical properties of brain extracellular space explored with ion-selective microelectrodes, integrative optical imaging and related techniques. In: Michael AC, Borland LM, editors. Electrochemical methods for neuroscience: CRC Press LLC; 2007. p. 167-204.

35.   Sigma-Aldrich. http://www.sigmaaldrich.com/etc/medialib/docs/Sigma/Product_Information_Sheet/1/p7668pis.Par.0001.File.tmp/p7668pis.pdf.

36.   Johnson RE, Jr., Dettre RH. Wettability and contact angles. Surface Colloid Sci. 1969;2:85-153.

37.   Neumann AW, Good RJ. Techniques of measuring contact angles [in surface studies]. Surf Colloid Sci. 1979;11:31-91.

38.   BDBiosciences. http://www.bdbiosciences.com/ptProduct.jsp?ccn=354248.

39.   Weston SA, Parish CR. New fluorescent dyes for lymphocyte migration studies: Analysis by flow cytometry and fluorescence microscopy. J Immunol Methods. 1990;133:87-97.

40.   Giordano G, Hong S, Faustman EM, Costa LG. Measurements of cell death in neuronal and glial cells. Methods Mol Biol 2011;758:171-8.

41.   Corish P, Tyler-Smith C. Attenuation of green fluorescent protein half-life in mammalian cells. Protein Eng. 1999;12:1035-40.

Figure 1. (A) Schematic representation of the decal-transfer method used to pattern hydrophobic paraffin films onto PET-based mesh sheets. (B) General scheme for the seeding of hydrogel-suspended cells on multi-zone supports. (C) Images of multi-zone PET-based mesh sheets with paraffin decal-transferred barriers and multi-zone paper with wax-printed barriers. Micrographs show the interface of the zone and the hydrophobic barriers of multi-zone paper and mesh.

Figure 2. Qualitative comparison of optical micrographs: image resolution of CiGiM and CiGiP for different concentrations of MDA-MB-231 cells. Cells were seeded in Matrigel and cultured for 12 hours to form stable cell-laden, gelled layers in the mesh. The dark "borders" are the PET threads that support the cell-laden gels. Scheme showing that Matrigel and cells form a continuous sheet through openings and threads of the PET-based mesh.

Figure 3. (A) Scheme summarizing the stacking of multi-zone sheets of CiGiM and CiGiP to generate 3D cell cultures with collective millimeter-scale thicknesses (9 layers × 200 μm thick/layer = 1.8 mm thick). We spotted 120,000 cells into each of the central nine zones of each layer. The generated stack was cultured for 9 days before de-stacking and analysis. A single layer (SL) containing the same number of cells in each zone was also cultured in parallel as a control. (B) Scheme for the conversion of non-fluorescent calcein-AM to fluorescent calcein by esterases present in viable cells. (C) Scanned images of the zones after disassembly of the stacked cultures of MDA-MB-231 cells. The grayscale intensities represent the fluorescence of calcein generated from the hydrolysis of calcein-AM by the intercellular esterase of viable cells. (D) Graph depicting the calcein intensity profile of mesh and paper. Intensity values from each zone were subtracted by the background intensity (empty zones where no cells were spotted),

and normalized by the intensity of L1. (E) Line scans show the distribution of the calcein intensity across the diameter of the zones of L6 in PET-based mesh and paper-based supports. (Inset) Image showing the zones of L6 The horizontal bars (8 mm) represent the areas measured to generate the line scans in (E).

Figure 4. (A) Confocal fluorescence images of MDA-MB-231-GFP cells showing the change of cell morphology (from spindle-shaped to round as cells were depleted of oxygen in the stacked culture (i.e. from L1 to L9). The control contained the same initial concentration of cells but cultured as a single layer for 9 days. (B) Enlarged images of the samples from the different layers to view cells at higher resolutions. Green fluorescence arises from the GFP expressed by the MDA-MB-231 cells and blue fluorescence arises from the binding of DAPI (4, 6-diamidino-2-phenylindole) to nucleic acids in the cells. (C) Histogram showing the average number of viable cells found in the zones of CiGiM from L1 to L9. Standard deviations were calculated based on nine replicates (n=9). Dotted line represents the initial density for each zone (120,000 MDA-MD-231-GFP cells/zone).

Figure 5. Invasion set-up for MDA-MB-231 cells using multi-zone, polymer-based sytem. (A) Scheme for the invasion set-up. Sheets of the multi-zone mesh sheets were stacked such that only one layer contained the cells ("cell-containing layers"), while the rest of the layers only contained Matrigel ("gel-only layers"). In layers which contain cells, we seeded a suspension of MDA-MB-231 cells in Matrigel with an initial seeding concentration is 120,000 cells/zone. The layers were stacked on top of a cellulose acetate, and cultured for 7 days prior to analysis. (B) Scanned images of calcein-stained zones of CiGiM from L1 to L4 after 7 days of culture and de-stacking. (C) Histogram showing the number of viable cells present in each layer after 7 days of

culture as a stack. Standard deviations were calculated based on three replicates (n=3). The black

box represents the number of cells initially seeded in the "cell-containing layer" at the start of the
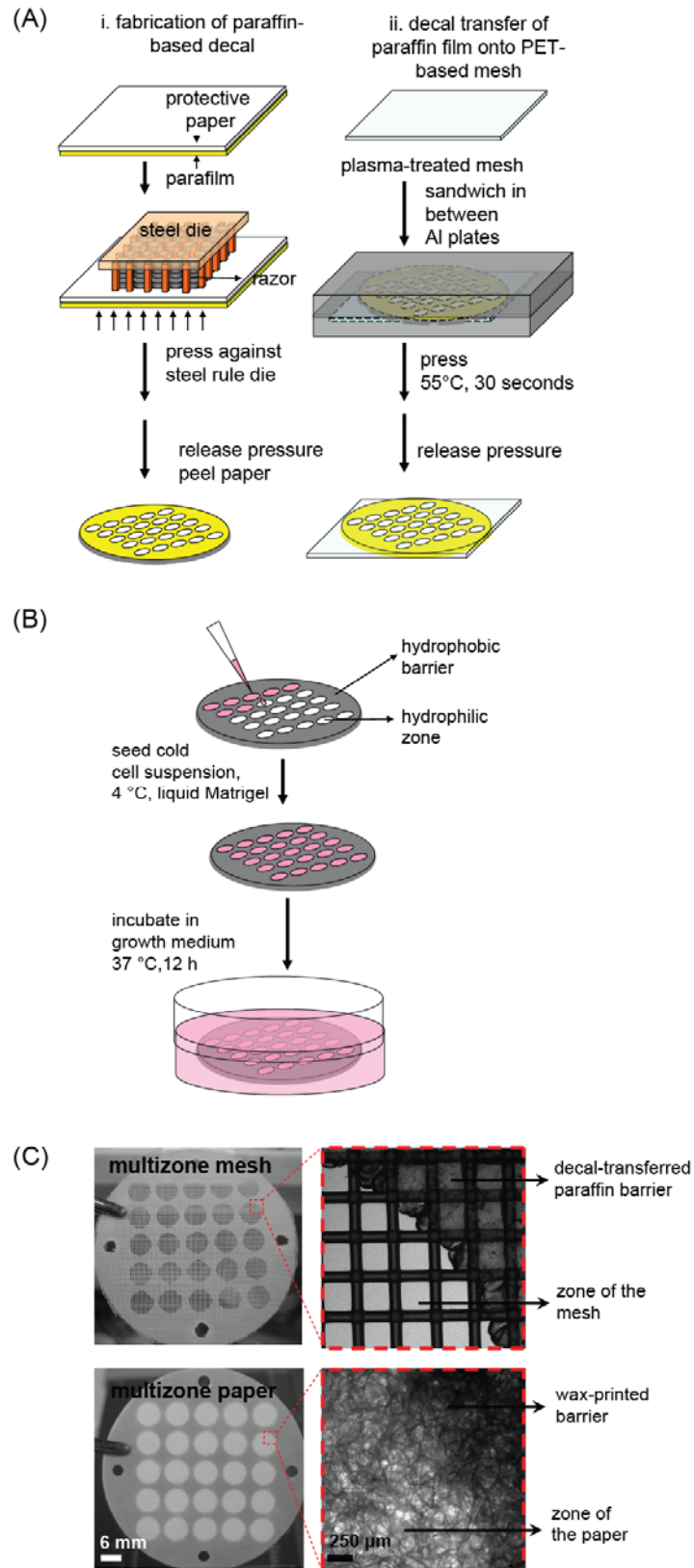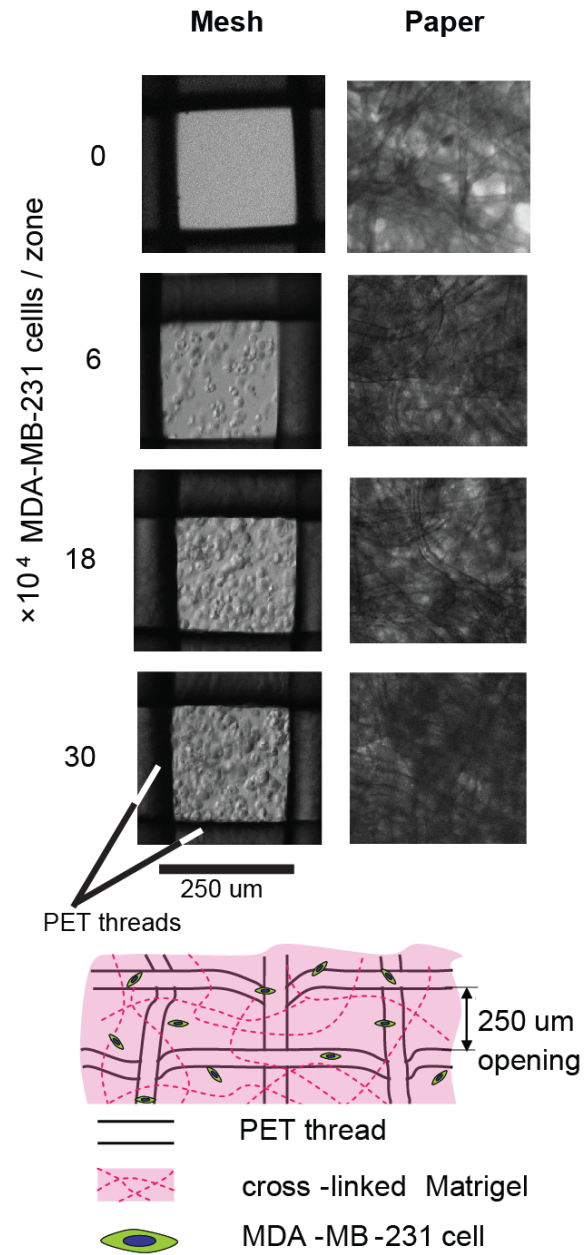
experiment.

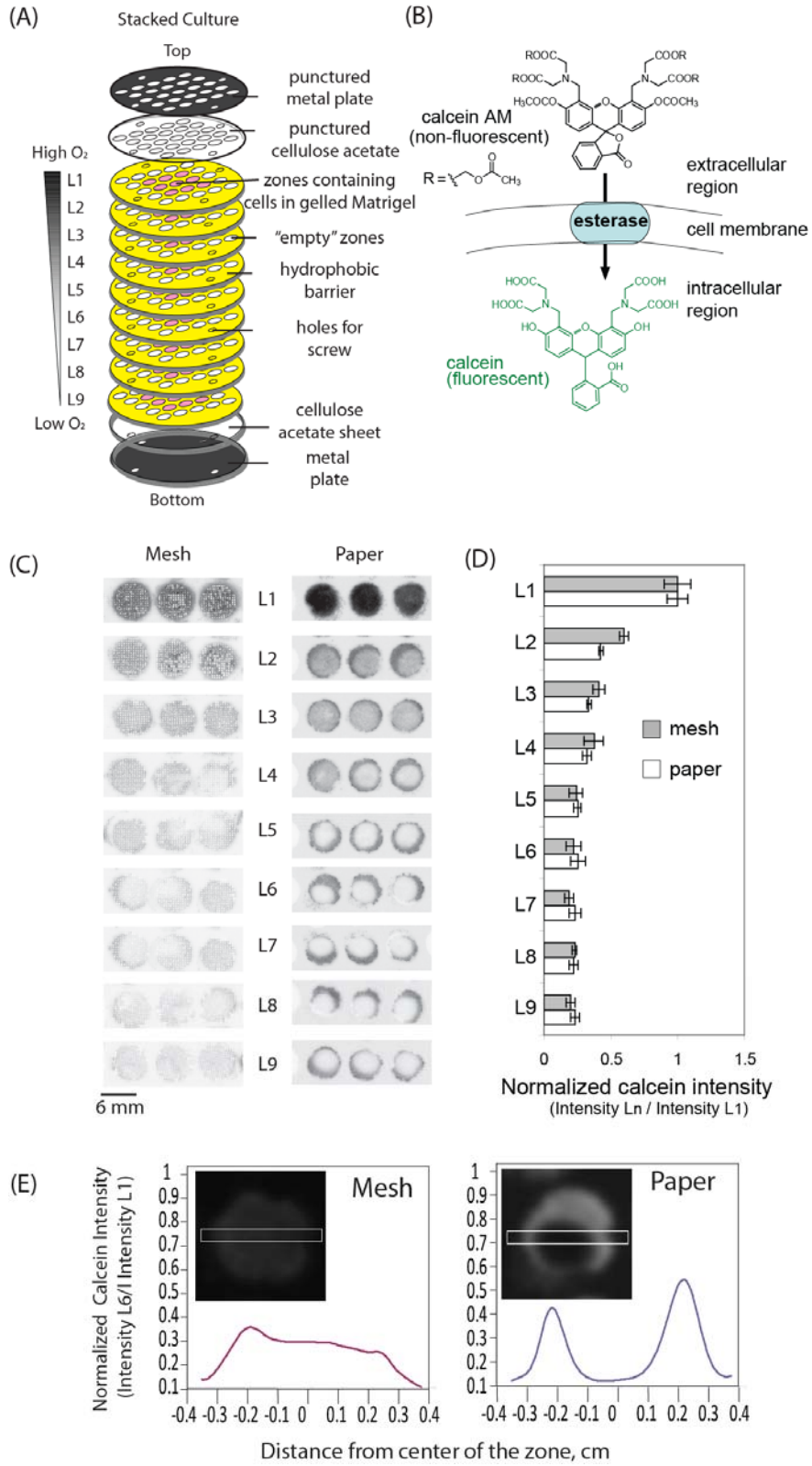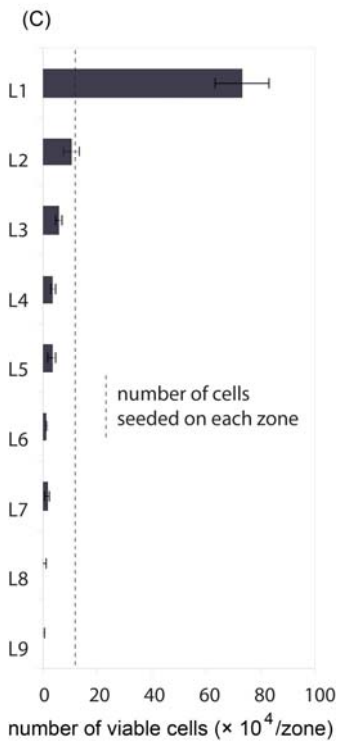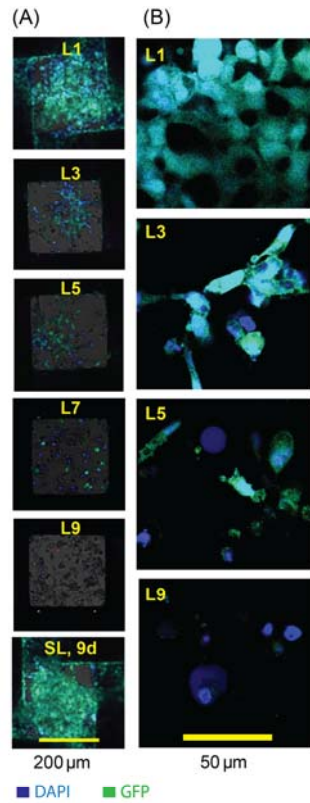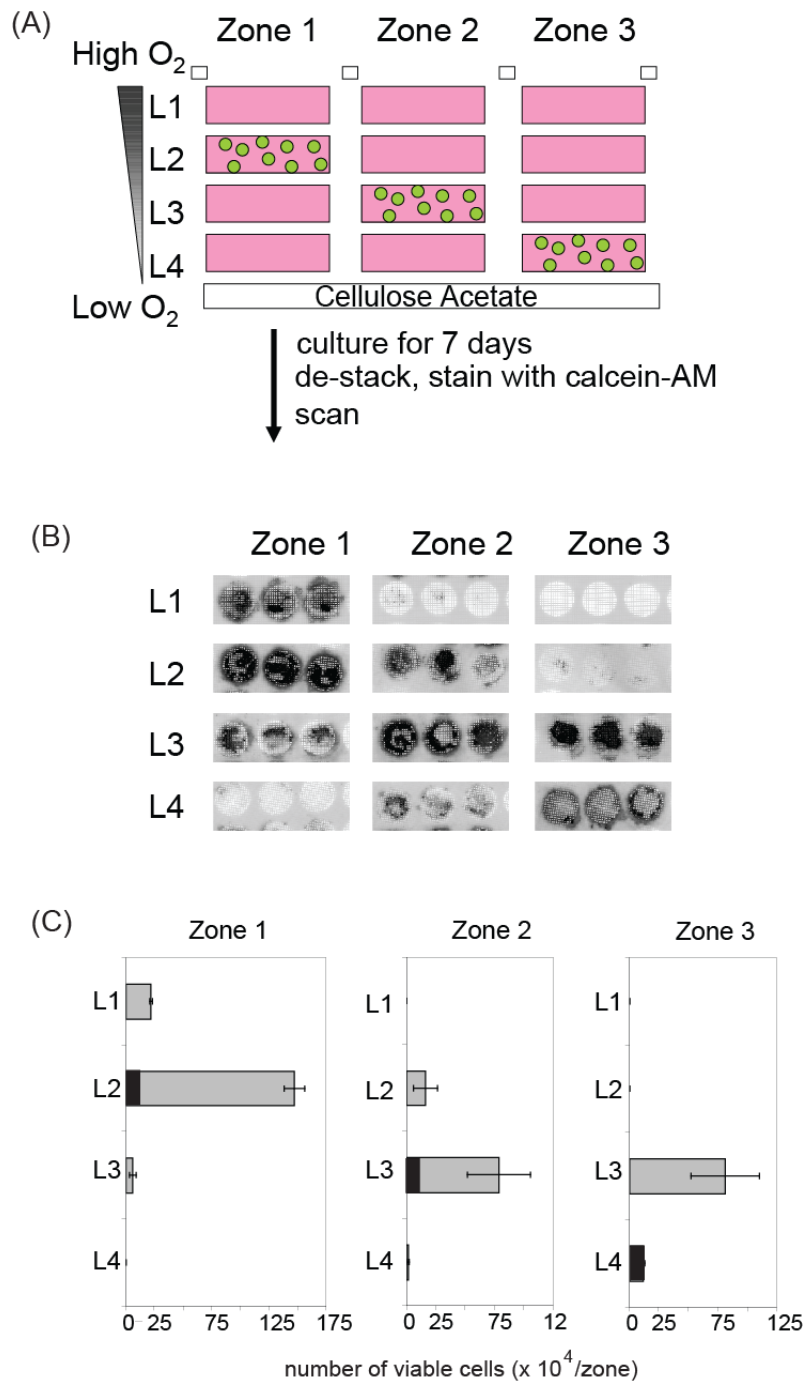**Figure 1.** *Simon et. al.*

Figure 2. *Simon et. al.*

Figure 3. *Simon et. al.*

Figure 4. *Simon et. al.*

Figure 5. *Simon et. al.*